Phys. Status Solidi RRL **8**, No. 3, 228–230 (2014) / **DOI** 10.1002/pssr.201308327

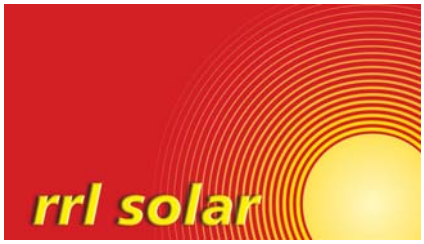

Radial distribution of iron in silicon crystals grown by Czochralski method from contaminated feedstock

Teimuraz Mchedlidze* **and Jörg Weber**

Technische Universität Dresden, 01062 Dresden, Germany

Received 10 December 2013, revised 7 January 2013, accepted 7 January 2013
Published online 10 January 2013

Keywords photovoltaics, silicon, iron, contamination, defects

* Corresponding author: e-mail teimuraz.mtchedlidze@physik.tu-dresden.de, Phone: +49 351463 37227, Fax: +49 351 463 37060

The radial distribution of iron in Cz-Si crystals grown from photovoltaic grade feedstock was analysed using deep level transient spectroscopy (DLTS). A high temperature annealing sequence followed by fast quenching to 273 K was used to transform iron silicide precipitates, formed after the crystal growth, to iron-containing species detectable by DLTS. The results suggest a homogeneous radial distribution of iron over the crystal. From comparison of as-grown and annealed samples, a strong suppression of iron precipitation close to the walls of the crystals becomes obvious and possible mechanisms of this phenomenon are discussed.

1 Introduction One of the strategies for the cost reduction of the solar cell fabrication suggests employment of cheap, low-purity feedstock for the crystal growth. It is supposed that the relevant degradation of the crystal quality could be amended by proper tailoring of the solar cell fabrication process [1]. Iron remains the most abundant and simultaneously most dangerous impurity for Si-based solar cells [2]. Detrimental influence of iron contamination could be minimised by proper gettering procedure [3]. Correct knowledge about the *total* iron content and its radial distribution inside the as-cut wafers is essential for proper modifications of solar cell fabrication processes. Despite the obvious importance of the topic, the present authors were able to find only a single publication related to the radial distribution of iron in as-grown Cz-Si crystals [4].

Various methods were used for detection and determination of the iron concentration in Si [5]. Limitations of the methods usually are related to insufficient detection limits, to destructiveness, or to a selective sensitivity to specific forms of Fe in Si. As an example, the method based on the lifetime measurements (LT) of minority charge carriers and deep level transient spectroscopy (DLTS) have the proper sensitivity range for measurements of photovoltaic-grade Si (PV-Si), but are unable to detect iron silicide precipitates, that contain most of iron atoms after the crystal growth. Contrary, the methods providing total iron content in Si samples are destructive, expensive and are not sufficiently sensitive.

The aim of the present work was establishing a simple and reliable method to convert all iron in the PV-Si to the species detectable by DLTS. Later the method was applied for defining the radial distribution of Fe in Cz-Si crystals.

2 Samples and experimental Silicon wafers, 150 µm thick, were cut-out at ~$\frac{3}{4}$ of the length of three 156 mm diameter crystals, labelled *A*, *B* and *C*. The crystals for the study were grown in standard Cz-Si crystal growth process by Bosch Solar Energy AG using differently mixed Si feedstock. The crystals were doped by boron to obtain a resistivity in the range of 3–6 Ω cm. Results of the analyses of Fe content in the centre of the as-cut wafers by various experimental methods were already presented [6]. The large scatter in the reported iron-content values between the results obtained by LT, DLTS and the inductively-coupled plasma mass-spectroscopy (ICPMS) methods are related to the insensitivity of the former two methods to iron atoms precipitated in the bulk of Si. On the other hand the detection limit of Fe content in Si by the ICPMS method was ~3×10^{13} cm^{-3}.

To detect the total iron content in the samples by the DLTS method, we decided to subject the as-grown samples to high-temperature annealing followed by fast quenching (HTAQ). Dissolution of iron silicide precipitates in Si could be performed at a temperature T_a, where the Fe solubility limit in Si is larger than its content in the samples. For this the sample has to be kept at T_a for a sufficient time t_a for total dissolution of the precipitates. As a result Fe atoms are transferred to the interstitial positions (Fe_I) in the Si lattice. The parameters for the HTA, i.e. T_a and t_a, could be determined experimentally by increasing the values of both parameters until the saturation of the resulting Fe_I concentration will be reached. For quenching of Fe atoms at interstitial sites and avoiding formation of Fe precipitates and/or other Fe-containing complexes, the samples should be quenched from the T_a to $T < 100$ °C [5]. In case of the proper quenching speed one should obtain a concentration of Fe_I in the quenched sample identical to the Fe solubility in Si at T_a. After quenching in p-type Si Fe_I pairs with B to form FeB [5]. Since DLTS is equally sensitive to Fe_I and FeB, this transformation does not create an obstacle for proper determination of Fe concentration in the quenched samples.

To establish proper HTAQ parameters and check the level of unintentional background Fe contamination in the process we performed experiments using electronic grade p-type FZ-Si and Cz-Si samples and samples prepared from the *A* type wafers. After RCA cleaning step [7], a sample was sealed in an RCA cleaned quartz capsule filled with noble gas (Ar or He) at low pressure. The capsule was later inserted to a specially designed furnace with vertically aligned annealing tube, heated to the specified temperature T_a. After the annealing duration t_a the capsule was dropped to a vessel with iced water. The time necessary for the capsule to reach the water level from the annealing location was ~1 sec. From these experiments we determined the reasonable parameters of the HTAQ treatment as $T_a = 950$ °C and $t_a = 30$ min.

Initial samples, $10 \times 5 \times 0.15$ mm^3 in size, were cut out from the locations at the rims of the wafers (samples *AE*, *BE* and *CE*) and at 55 mm distance from the rims (samples *AM*, *BM* and *CM*). For the reference (*R*) we used similar sized samples cut from p-type FZ-Si electronic grade wafer with resistivity 2.5 Ω cm. The samples intended for the HTAQ process were subjected to RCA cleaning procedures in the same batch process, and were sealed in separate quartz capsules. Subsequently, each capsule was subjected to the HTAQ process with the parameters presented above. The labels of the samples subjected to the HTAQ process will finish on "*Q*" (e.g. *AEQ*), while labels of the samples in as-grown state – with "*G*" (e.g. *AMG*); "*#*" in the label will be used as a wildcard.

For DLTS measurements the untreated and quenched samples were etched in $HF + HNO_3$ (1:5) solution for 1 min. Subsequently, 50 nm thick Al dots with 0.5–1.8 mm^2 area were evaporated on the surface of the samples for the Schottky contacts. Ohmic contacts were formed by rubbing-in InGa eutectic solution to the reverse surface of the samples.

DLTS measurements were performed by means of a standard lock-in system working at the capacitance testing frequency of 1 MHz. Principles of the method and the system were previously described [8]. Cooling of a sample was done by immersion in a dewar with liquid He and a temperature controller maintained necessary temperature in the range of 35–300 K.

3 Results and discussion The distribution of FeB trap densities near to the wafer rims in the *##G* and *A#Q* samples, determined from the DLTS measurements, are presented in Fig. 1. A weaker peak (~1/10 of the FeB peak intensity) of unknown origin paralleled the behaviour for the intensity of the FeB peak in *#EG* samples. From the DLTS measurements the parameters of the related trap, labelled H105, corresponded to an energy level position in the band gap $E_{H105} = E_V + 0.2$ eV and an apparent carrier capture cross section of $\sigma \approx 2.2 \times 10^{-15}$ cm^2. No FeB or H105 peaks were detected for *#MG* samples. Occasional weak peaks, detected in several spectra, were attributed to dislocations and/or to oxide precipitates.

No traps were detected in the *RG* sample and 1.2×10^{12} cm^{-3} FeB traps – in the *RQ* sample (Fe contamination level resulted from the HTAQ). This background value was subtracted from the FeB trap densities detected in other quenched samples. In the samples subjected to the HTAQ, the radial dependence for the FeB-related peak intensities was absent at the achieved accuracy level. A correlation of the FeB densities for *##Q* samples with those in near-to-the-rim locations of *#EG* samples is shown in Fig. 2, where the dashed line sketches a one-to-one correspondence. Signals from H105 traps were not detected in the spectra of the *##Q* samples. Instead, a peak corresponding to a trap labelled H158 with parameters $E_{H158} = E_V + 0.26$ eV and $\sigma \approx 1 \times 10^{-17}$ cm^2 was detected. The density of the H158 traps was similar for all samples and amounted to $3–5 \times 10^{11}$ cm^{-3}. Traps labeled H205 were detected only in the *CMQ* sample ($E_{H205} = E_V + 0.38$ eV

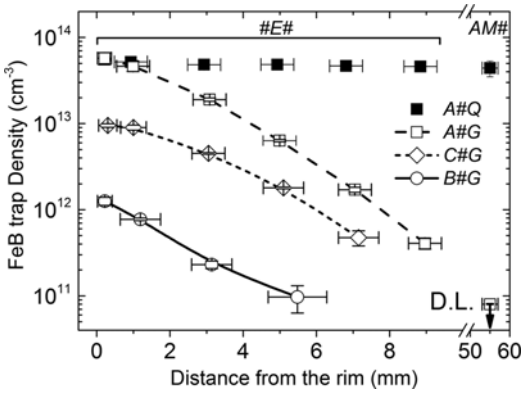

Figure 1 Distribution of FeB traps in *##G* and *A#Q* samples. Lines are guides to the eye. In *#MG* samples FeB traps were under the detection limits (D.L.).

and $\sigma \approx 1.3 \times 10^{-16}$ cm^2). The estimated density of H205 was ~4×10^{11} cm^{-3}.

The absence of a radial dependence for the FeB density for the quenched samples unambiguously suggests that after the crystal growth Fe atoms were equally distributed along the crystal radius. Apparently, during the after-growth cooling, iron precipitation was suppressed near to the rims of the crystals, where the large FeB trap density was detected later. Moreover, direct correspondence of Fe density values at the rim locations to those in the samples after quenching (see Fig. 2) suggests that the precipitation was completely blocked at the rims of the crystals despite the differences in the total iron content between *A–C* samples. A possible mechanism of such a suppression presents substantial interest for Fe-related defect engineering, since the prevention of precipitation in the whole crystal will facilitate Fe gettering during solar cell fabrication process [3].

Several mechanisms of the phenomenon can be proposed from the observed character of FeB density gradient near to the rims of the crystals (see Fig. 1). Note, that in-diffusion of Fe atoms from the furnace atmosphere and/or walls of the growing crystal, like it was proposed in [4], can be excluded. First, Fe atoms, if diffused at high temperatures, should precipitate during cooling of the monocrystal. Second, it was shown that the total iron concentration was independent from radial position. Third, inside the in-diffusion model it will be difficult to find a reason for different levels of in-diffused Fe density for the similarly grown *A–C* crystals. Temperature gradients, causing an effect similar to quenching during the crystal cooling process, could also be excluded due to high thermal conductivity and slow cooling rates of the crystals after the growth.

Probably additional information could be obtained from the investigation of the H105 traps that parallel the behaviour of FeB concentration near to the crystal rims. Our preliminary measurements revealed a poor thermal stability of the traps: they annealed out after 30 min treatment of *#EG* samples at 150 °C. This suggests that H105 traps were formed at the last stages of crystal cooling, probably together with FeB formation. Simultaneously with vanishing of that trap due to annealing, the concentration of the FeB increased. The increment value of the FeB peak doubled the value of the H105 peak in the starting sample, suggesting that two Fe atoms were contained in the H105 trap.

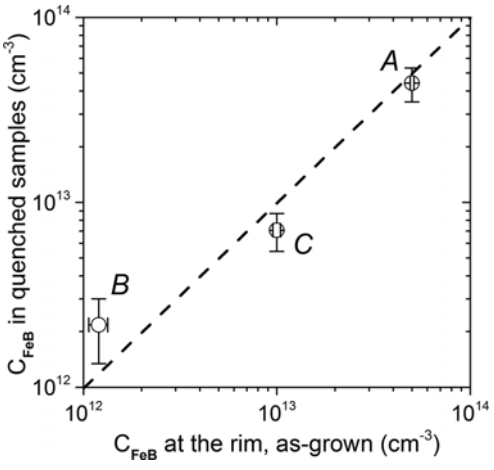

Figure 2 Correlation of the FeB trap densities in the *A–C* crystals. On *x*-axis: the densities at near-to-the-rim locations in untreated samples; on *y*-axis: the averaged densities in the quenched samples.

Radial distribution of various ingrown defects in Cz-Si crystals is widely discussed already for long time (see e.g. [9, 10] and references therein). Various effects from interaction of Fe atoms with point and extended defects were also reported [5]. We propose that the suppression of Fe precipitation is related to a gradient in the density of some ingrown defects or defect complexes near to the crystal rim. Further investigations will be necessary to clarify the origin of the observed phenomena.

In summary, high temperature annealing followed by fast quenching procedure was applied to detect total iron concentration in various radial locations of Cz-Si wafers by DLTS. Iron atoms were equally distributed along the radius of the wafers in the limits of the experimental error. Nearly total suppression of Fe precipitation in Cz-Si was detected at the rim of the as-grown crystals with total iron content in the range 10^{12}–10^{14} cm^{-3}. The level of precipitation strongly increased to the centre of the crystal and at a distance of ~6–10 mm from the wafer rims almost all Fe atoms were precipitated. Determining the mechanism of the phenomenon will permit finding new strategies for Fe gettering in Si. The mechanism also presents a fundamental interest for understanding of iron behaviour in silicon.

Acknowledgements The authors would like to thank the colleagues from Bosch Solar Energy AG for the growth of the crystals and preparation of the wafers. The work was supported by the German Ministry for Education and Research under contract 03SF0398K (xμ-Material) in the framework of the Excellence Cluster Solar Valley Central Germany.

References

[1] J. Hofstetter, J. F. Lelièvre, C. del Canizo, and A. Luque, Mat. Sci. Eng. B **159–160**, 299 (2009).
[2] D. P. Fenning, J. Hofstetter, M. I. Bertoni, G. Coletti, B. Lai, C. del Cañizo, and T. Buonassisi, J. Appl. Phys. **113**, 044521 (2013).
[3] V. Vähänissi, A. Haarahiltunen, H. Talvitie, M. Yli-Koski, and H. Savin, Prog. Photovolt.: Res. Appl. **21**, 1127 (2013).
[4] D. Gilmore, T. Arahori, M. Ito, H. Murakami, and S. I. Miki, J. Electrochem. Soc. **145**, 621 (1998).
[5] A. A. Istratov, H. Hieslmair, and E. R.Weber, Appl. Phys. A **70**, 489 (2000).
[6] K. Lauer, C. Möller, K. Neckermann, M. Blech, M. Herms, T. Mchedlidze, J. Weber, and S. Meyer, Energy Procedia **38**, 589 (2013).
[7] W. Kern, J. Electrochem. Soc. **137**, 1887 (1990).
[8] G. L. Miller, D. V. Lang, and L. C. Kimerling, Annu. Rev. Mater. Sci. **7**, 377 (1977).
[9] T. Abe and T. Takahashi, J. Cryst. Growth **334**, 16 (2011).
[10] V. V. Voronkov and R. Falster, J. Cryst. Growth **351**, 115 (2012).